Wearable Electronics Hot Paper

Deutsche Ausgabe: DOI: 10.1002/ange.201506142
Internationale Ausgabe: DOI: 10.1002/anie.201506142

Realizing both High Energy and High Power Densities by Twisting Three Carbon-Nanotube-Based Hybrid Fibers

*Ye Zhang, Yang Zhao, Xunliang Cheng, Wei Weng, Jing Ren, Xin Fang, Yishu Jiang, Peining Chen, Zhitao Zhang, Yonggang Wang, and Huisheng Peng**

Abstract: *Energy storage devices, such as lithium-ion batteries and supercapacitors, are required for the modern electronics. However, the intrinsic characteristics of low power densities in batteries and low energy densities in supercapacitors have limited their applications. How to simultaneously realize high energy and power densities in one device remains a challenge. Herein a fiber-shaped hybrid energy-storage device (FESD) formed by twisting three carbon nanotube hybrid fibers demonstrates both high energy and power densities. For the FESD, the energy density (50 mWh cm^{-3} or 90 Wh kg^{-1}) many times higher than for other forms of supercapacitors and approximately 3 times that of thin-film batteries; the power density (1 W cm^{-3} or 5970 W kg^{-1}) is approximately 140 times of thin-film lithium-ion battery. The FESD is flexible, weaveable and wearable, which offers promising advantages in the modern electronics.*

The increasing energy and power requirement for the next-generation wearable and flexible electronics stimulates more and more efforts to explore new energy-storage devices. In practical applications, both high energy and high power outputs are required. However, it is difficult for an energy-storage device to simultaneously achieve high energy and high power output. For instance, the fuel cells and lithium-ion batteries (LIBs) demonstrate high energy densities but low power densities, while the supercapacitors show high power densities but very low energy densities. Some efforts have been made to synthesize novel electrode materials to enhance the power and energy densities.[1–3] However, the methods are complex and high-cost with limited improvements. How to realize both high energy and high power densities in one device still remains a challenge.

On the other hand, flexible and wearable electronic textiles represents an emerging and promising area, which has been studied in a variety of fields including smart clothes and electronic skins.[4–13] To this end, it is desirable to integrate efficient power systems that are lightweight, flexible and weaveable. Several attempts have been thus made to explore flexible LIBs and supercapacitors in a fiber shape.[14–18] However, similar to the conventional planar energy storage device,[19,20] these drawbacks of low power densities in batteries and low energy densities in supercapacitors make them unavailable for various electronic facilities where both high energy and high power densities are simultaneously required.

Herein, we have designed a general and effective twisted structure to simultaneously achieve both high energy and power densities. This novel fiber-shaped hybrid energy storage device (FESD) is fabricated by twisting carbon nanotube (CNT)/ordered mesoporous carbon (OMC), CNT/$Li_4Ti_5O_{12}$ (LTO), and CNT/$LiMn_2O_4$ (LMO) hybrid fibers together (Figure 1 a), which integrated the properties of the lithium-ion battery and the supercapacitor to give both high energy and power densities. The one-dimensional fiber shape offers advantages, for example, it can be woven into various flexible electronic textiles or other flexible structures.

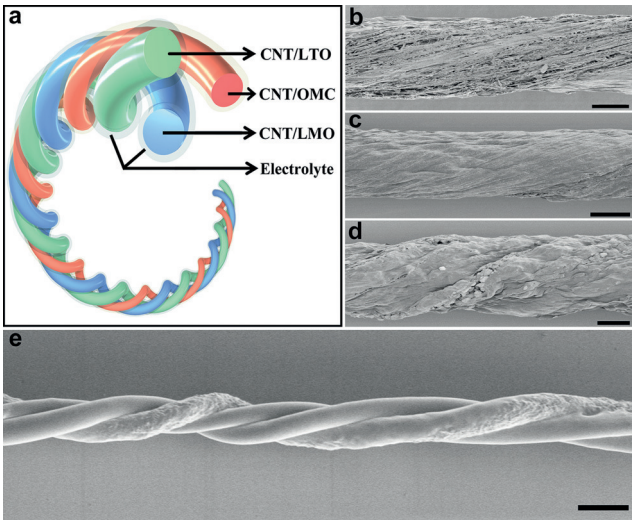

Figure 1. a) Schematic illustration to the structure of the FESD. b)–d) SEM images of the CNT/OMC, CNT/LTO, and CNT/LMO hybrid fibers, respectively. e) SEM image of an FESD. Scale bars: 50 μm (b–d), 300 μm (e).

Spinnable CNT arrays were first synthesized by chemical vapor deposition and the aligned CNT sheets were dry-drawn

[*] Y. Zhang, Y. Zhao, Dr. X. Cheng, Dr. W. Weng, J. Ren, X. Fang, Y. Jiang, P. Chen, Z. Zhang, Prof. H. Peng
State Key Laboratory of Molecular Engineering of Polymers
Collaborative Innovation Center of Polymers and Polymer Composite Materials, Department of Macromolecular Science and Laboratory of Advanced Materials
Fudan University, Shanghai 200438 (China)
E-mail: penghs@fudan.edu.cn
Prof. Y. Wang
Department of Chemistry and Shanghai Key Laboratory of Molecular Catalysis and Innovative Materials, Institute of New Energy, iChEM (Collaborative Innovation Center of Chemistry for Energy Materials)
Fudan University, Shanghai 200438 (China)

Supporting information for this article is available on the WWW under http://dx.doi.org/10.1002/anie.201506142.

from the array (Supporting Information, Figure S1).[21,22] The OMC nanoparticles with a diameter of approximately 1 μm (Figure S2) were then incorporated into the CNT sheets, which were then rolled into a CNT/OMC hybrid fiber. Figure 1b shows a typical scanning electron microscopy (SEM) image of the CNT/OMC fiber electrode with a diameter of approximately 100 μm. The LTO and LMO nanoparticles were synthesized by solid-state and hydrothermal methods,[23,24] respectively, and X-ray diffraction patterns indicated a spinel structure for both of them (Figure S3 and S4). The nanoparticles were irregular in morphology (Figure S5 and S6), and the average sizes were 113 nm for LTO and 131 nm for LMO (Figure S7 and S8). Active LMO and LTO materials were incorporated into the CNT fiber to produce CNT/LMO and CNT/LTO hybrid fibers by a co-spinning process. The main preparation included the coating of active nanoparticle suspensions onto the CNT sheet, then a scrolling process to transform the two-dimensional sheet into a one-dimensional fiber. The weight percentages of the active materials were controlled by varying the concentration of the suspension. The CNT/LTO and CNT/LMO hybrid fibers also exhibited uniform diameters of 80 and 115 μm, respectively (Figure 1c,d). Note that OMC, LTO, and LMO nanoparticles have been stably incorporated among aligned CNTs in the hybrid fibers (Figure S9–S13).

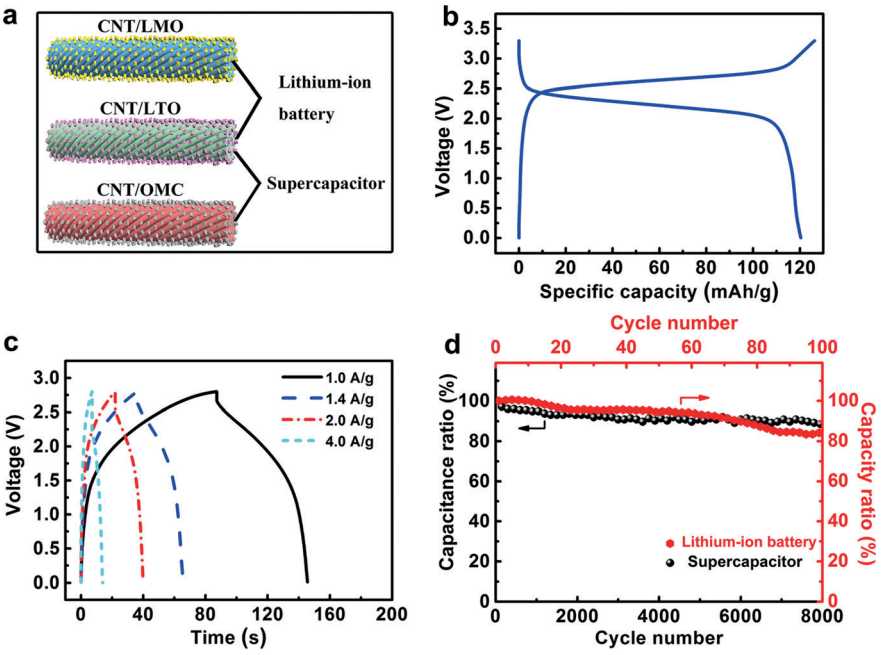

Figure 2. Electrochemical performance of the FESD separately acting as a lithium-ion battery and supercapacitor. a) Schematic illustration to constitution of the LIB and supercapacitor segments. b) Charge and discharge profiles of the LIB segment at a current density of 0.5 $A g^{-1}$. c) Galvanostatic charge–discharge curves of the supercapacitor segment at increasing current densities. d) Cyclic performance of the LIB and supercapacitor segments.

The CNT/OMC, CNT/LTO, and CNT/LMO hybrid fibers were then coated with a thin layer of lithium bis(trifluoromethane)sulfonamide (LiTFSI)/succinonitrile (SCN)/poly(ethyleneoxide) (PEO) gel electrolyte, and finally twisted to produce the FESD (Figure S14). The gel electrolyte was uniformly coated on the fiber electrodes and the three fiber electrodes could be closely and stably intertwined (Figure 1e). The gel electrolyte not only functioned as a conducting medium, but also acted as a separator to prevent short circuits. Compared with the traditional planar structure, the combined one-dimensional and twisted structure makes it available to integrate the lithium-ion battery and supercapacitor in one device. The resulting FESD was also lightweight with a linear weight density of 0.84 $g m^{-1}$.

Figure 2a schematically shows how the FESD can act as both LIB and supercapacitor. The CNT/LTO, CNT/LMO hybrid fibers and gel electrolyte formed the LIB part, and the reactions during the charge and discharge processes are listed in Equations (1) and (2):

$$LiMn_2O_4 \leftrightarrow 2\,MnO_2 + Li^+ + e^- \quad (1)$$

$$Li[Li_{1/3}Ti_{5/3}]O_4 + Li^+ + e^- \leftrightarrow Li_2[Li_{1/3}Ti_{5/3}]O_4 \quad (2)$$

During the charge process, lithium ions are leave the $LiMn_2O_4$ lattice in the positive electrode and then transfer to the electrolyte and insert in the $Li_4Ti_5O_{12}$ lattice in the negative electrode. Meanwhile, the electrons flow to the negative electrode through the external circuit.[25] The process is reversed in the discharge process.

The balancing mass ratio of the LTO and LMO was designed to be 1/2 to achieve a matchable capacity. We further investigated the electrochemical performances with different LTO contents in the hybrid fiber. As shown in Figure S15, the specific capacities first increased with the increasing LTO weight percentage from 26% to 73% as a result of the high utilization of active materials; they then decreased with the further increase in the weight percentage as the nanoparticles could not be effectively incorporated inside the fiber. Optimal weight percentages of LTO and LMO in the hybrid fibers were 73% and 86%, respectively, and they were used in the devices in the following discussion. The typical voltage profiles of the LIB segment at a voltage range of 0–3.3 V are shown in Figure 2b. The average discharge plateau voltage occurred at approximately 2.3 V that corresponded to the voltage difference between the CNT/LTO and CNT/LMO electrodes. The specific capacity was calculated as 120.5 $mAh g^{-1}$ at the current density of 0.5 $A g^{-1}$ at the first cycle and can be maintained over 80% after 100 cycles (Figure 2d). The rate capacity of the LIB segment at increasing current densities was also carefully investigated (Figure S16). The specific capacity could be maintained at 113.2 $mAh g^{-1}$ at 1 $A g^{-1}$ and 99.6 $mAh g^{-1}$ at 1.5 $A g^{-1}$. The battery segment showed an energy density of 98.6 $Wh kg^{-1}$

and a power density of 445.4 W kg^{-1} at the current density of 0.5 A g^{-1}.

The CNT/LTO electrode was also paired with the CNT/OMC electrode to function as a supercapacitor. The electrochemical performance of the supercapacitor segment was investigated by a galvanostatic charge–discharge test between 0 and 2.8 V. To find the optimal weight percentage of OMC in the hybrid fiber, we compared the specific capacitances with increasing OMC weight percentages (Figure S17). The specific capacitances increased with increasing weight percentage from 23% to 46%. They slightly decreased with further increase in the OMC weight percentage as a result of the increasing electrical resistance. In this case, an optimal weight percentage of OMC in the hybrid fiber was 46% and has been used in the devices in the following discussion. Figure 2c shows the charge–discharge curves at increasing current densities. The nearly symmetric shape is maintained with increasing current densities from 1 to 4 A g^{-1}, indicating that the supercapacitor can perform stably at a wide range of currents. The specific capacitance was 22.1 F g^{-1} at the current density of 1 A g^{-1} based on the whole weight of the CNT/LTO and CNT/OMC hybrid electrodes. To further investigate the stability of the supercapacitor, the specific capacitance was traced and maintained by 90.3% after 8000 cycles (Figure 2d). The supercapacitor segment showed an energy density of 8.04 W kg^{-1} and a high power density of 4136.7 W kg^{-1} at the current density of 4 A g^{-1}.

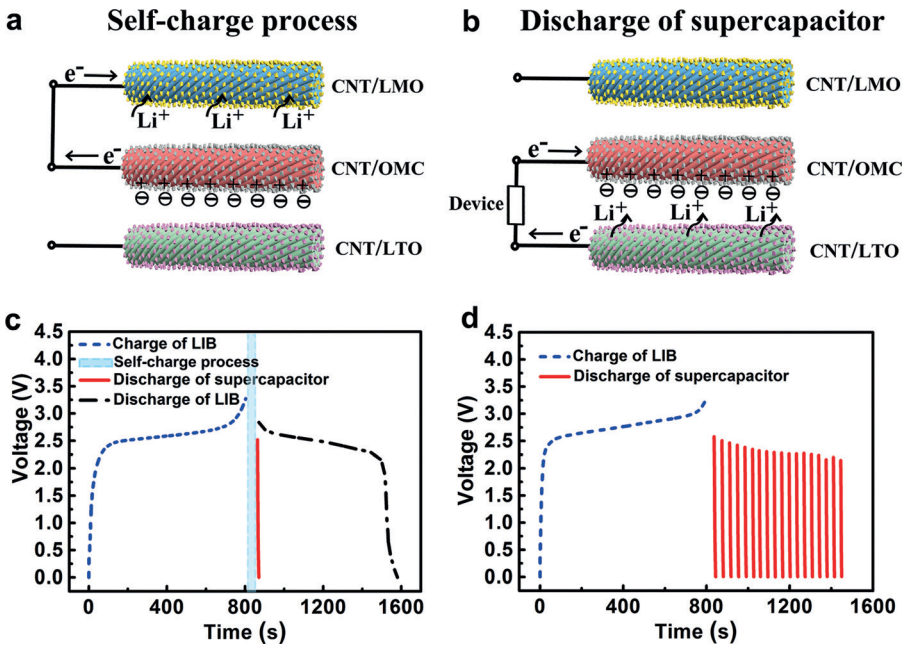

Figure 3. The design to achieve both high power and energy output. a), b) Schematic illustrations of the self-charge process and discharge of the supercapacitor segment. c) The charge and discharge curves of the FESD which was alternately discharged as a supercapacitor and a LIB. d) The charge and discharge behavior of an FESD in which the LIB and supercapacitor segments served as energy storage and output, respectively.

The two segments can function together to achieve various power outputs for practical applications. When an instant peak power output (e.g. Start flash before photographing) is required, the supercapacitor segment will work as the power output unit. In this case, the LIB segment works as the energy storage unit and the discharge of the LIB is used to charge the supercapacitor, which is called a self-charge process (Figure 3a). The working mechanisms are schematically shown in Figure S16. The CNT/LTO and CNT/LMO electrodes were first connected to charge the LIB segment. After the LIB was fully charged, the positive electrode was converted into MnO_2 through the deintercalation reaction [Eq. (1)] and the negative electrode was transformed to $Li_7Ti_5O_{12}$ [Eq. (2)] through the intercalation reaction. The CNT/LMO electrode and CNT/OMC electrode were then directly connected. Owing to the potential difference, electrons flowed from the CNT/OMC electrode to the CNT/LMO electrode, which resulted in the reactions in Equations (3) and (4):

$$OMC + x\,TFSI^- \rightarrow OMC^+||x\,TFSI^- + x\,e^- \quad (3)$$

$$2\,MnO_2 + x\,Li^+ + x\,e^- \rightarrow Li_xMn_2O_4 \quad (4)$$

According to Equations (3) and (4), the surfaces of the OMC adsorbed a lot of anions in the electrolyte (i.e., bis(trifluoromethane)sulfonamide ($TFSI^-$)), and simultaneously, some Li ions were intercalated into the MnO_2. The CNT/OMC electrode (i.e., $OMC^+||x\,TFSI^-$) was coupled with the lithiated negative electrode (i.e., $Li_7Ti_5O_{12}$) to form a supercapacitor (Figure 3b), and can display the high power character according to Equations (5) and (6):

$$OMC^+||x\,TFSI^- + x\,e^- \leftrightarrow OMC + x\,TFSI^- \quad (5)$$

$$Li_2[Li_{1/3}Ti_{5/3}]O_4 \leftrightarrow Li_{2-x}[Li_{1/3}Ti_{5/3}]O_4 + x\,Li^+ + x\,e^- \quad (6)$$

Figure 3c shows a whole charge–discharge process of the FESD. The LIB section was charged at the current density of 0.02 mA cm^{-1} and functioned as the energy storage unit with a charge energy density of 48.1 mWh cm^{-3} based on the whole volume of the three electrodes and 85.2 Wh kg^{-1} based on the total mass of the three electrodes. The CNT/LMO and CNT/OMC electrodes were directly connected to self-charge the supercapacitor for 30 seconds. After the self-charge, the voltage of the supercapacitor section rose to 2.5 V, and it worked as the high power output unit to discharge at the current density of 0.5 mA cm^{-1} with a power density of 1.07 W cm^{-3} or 5971.1 W kg^{-1}. The self-charging time was determined by the kinetics of Equations (3) and (4), which is a little longer than the discharging time. After the instant peak power output, the LIB section continued to discharge at a low current density of 0.02 mA cm^{-1} to provide a low and

stable power for a long time. The FESD exhibited the characteristics of both a supercapacitor and a LIB, and the combined advantages have been further investigated when it was alternately discharged as a supercapacitor and an LIB for 100 cycles (Figure S17). The capacity of the LIB segment could be maintained at 71.4% and the capacitance of the supercapacitor segment was sustained at almost 100% after 100 charge–discharge cycles, demonstrating a high cyclic performance. By virtue of this design, the FESD has various ways of power output and endowed them with properties for practical applications, for example, an instant peak power output can be provided to start a flash before photographing and a stable long power output to support the running of the camera.

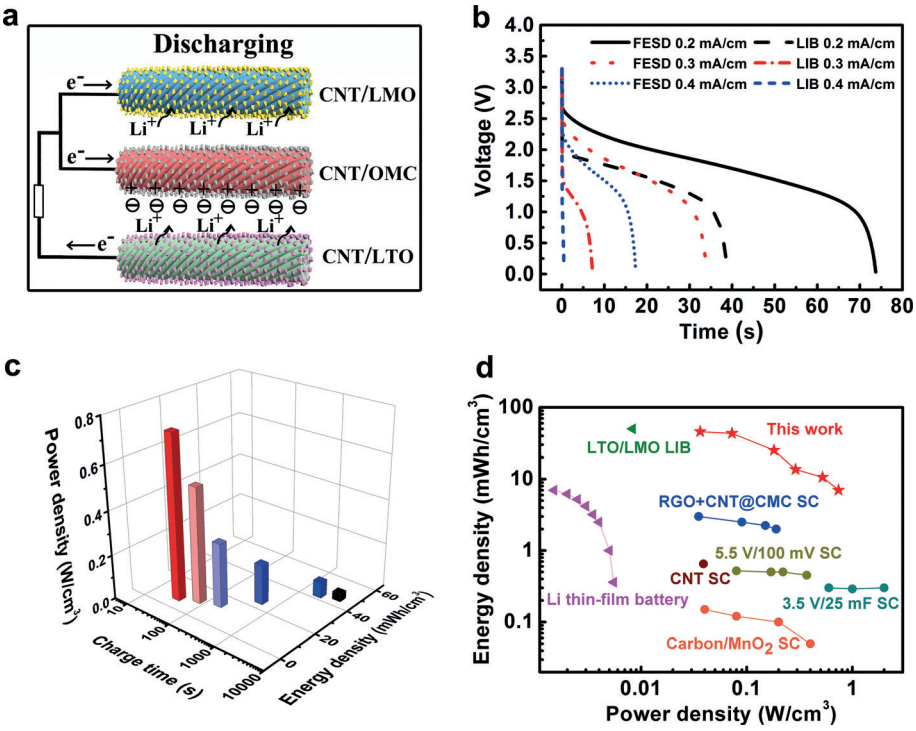

Figure 4. Electrochemical performances with both high volumetric energy and power densities in the FESD. a) Schematic illustration to the discharge process of the FESD in which the CNT/LMO and CNT/OMC electrodes were connected to work as positive electrodes. b) Comparison on discharge curves of the FESD and the LIB section at different current densities. c) Ragone plot (energy density versus power density versus charge time). d) Energy and power densities of the FESD and of reported energy storage systems CNT SC,[17] RGO + CNT@CMC SC,[27] commercially available supercapacitors (3.5 V/25 mF and 5.5 V/100 mF),[27,28] carbon/MnO_2 SC,[29] Li thin-film battery,[26] and planar LMO/LTO LIB.[30] SC = supercapacitor.

In addition, the pulse high power output can also be achieved by repeating the operations shown in Figure 3a and 3b. Through the self-charge process after each high power output, the energy stored in the LIB section flowed to the supercapacitor section, and then the supercapacitor section worked as the power output unit, so the FESD can continue to provide the pulse high power output. As shown in Figure 3d, after the first self-charge process, the voltage of the supercapacitor section was charged to 2.5 V, and then it was discharged at the current density of 0.5 mA cm^{-1} to provide a high power output of 1.07 W cm^{-3}. By repeating the self-charge process, the FESD can provide the pulse high power output 18 times and the operating voltage window was above 2.0 V after the last self-charge process. The total discharge energy density of the FESD was 31.26 mWh cm^{-3} and the energy efficiency (i.e., the ratio of discharge energy and charge energy) was 65%.

We further tested the electrochemical performance of the FESD under different current densities. As shown in Figure 4a, the CNT/LMO and CNT/OMC electrodes were connected to work as positive electrodes, and the CNT/LTO electrode serves as a common negative electrode. When the FESD was discharged at a stable low current density, the delithiated LMO obtained electrons along with Li ions in the intercalating reaction. Simultaneously, the OMC obtained electrons to deliver capacity. For the external circuit, electrons flowed from the CNT/LTO electrode to the CNT/LMO electrode and CNT/OMC electrode. When the FESD discharged at a high current density, electrons mainly flowed from the CNT/LTO electrode to the CNT/OMC electrode in the external circuit and the FESD principally demonstrated the characters of the supercapacitor, which was verified by the data plotted in Figure 4b. At a higher current density, the FESD demonstrated a much higher discharge voltage compared with the LIB section, while the LIB section without the CNT/OMC electrode cannot endure a current density of 0.3 mA cm^{-1}. These results indicated that, by introducing a CNT/OMC fiber electrode, the electrochemical performance of the FESD was much improved particularly at high currents.

To further demonstrate the performance of the FESD, a Ragone plot derived from the charge–discharge curves at various current densities is shown in Figure 4c and is compared with the previous reported energy storage systems (Figure 4d and S20). The FESD exhibited high power densities up to around 1 W cm^{-3} or approximately 5970 W kg^{-1}, which is about 140-times higher than the thin-film lithium-ion batteries.[26] The energy density of the FESD reached about 50 mWh cm^{-3} or approximately 90 Wh kg^{-1}, which is around 3-times that of the thin-film lithium-ion battery,[26] 6-times that of fiber-shaped supercapacitors based on RGO and CNT@CMC,[27] 35-times that of fiber-shaped supercapacitors based on CNTs,[17] 63-times that of commercially available supercapacitors (3.5 V/25 mF and 5.5 V/100 mF)[27,28] and 105-times of fiber-shaped supercapacitors based on carbon and MnO_2.[29]

The remarkable electrochemical performance of the FESD may be attributable to the following factors: First, owing to the excellent electrical and mechanical properties, the aligned CNT fiber serves as a skeleton to host active nanoparticles for electrical transport and physical support. No binder or metal substrate is needed, thus the weight and volume of the device is comparatively low and the usable specific energy density is increased compared with the conventional LIBs and supercapacitors. Second, the combined one-dimensional and twisted structure means any two of the three electrodes closely contacted, which is beneficial for the ionic transport between the electrodes. Most importantly, owing to the structure design of the FESD, the superiorities of high energy density in battery and high power density in supercapacitor are united together in one device.

The FESDs were flexible and could be bent into various shapes without damages in structure (Figure 5a and b). As shown in Figure S21, the twisted structure is maintained under bending because of the protection provided by the gel electrolyte. In addition, the charge and discharge curves remained almost unchanged after bending for 500 and 1000 cycles (Figure 5c). The FESDs can be twisted in three dimensions owing to its unique fiber shape, while thin-film LIBs and supercapacitors are generally deformable only under bending along one dimension. This FESD can be manufactured on a large scale, and the electrochemical performances are maintained on increasing the length from 10 to 200 mm (Figure S22). Moreover, the FESDs were also weaveable, and they had been woven into various flexible textiles, such as a knitted sweater (Figure 5d) and a glove (Figure 5e). As shown in Figure 5e, the FESD woven into a glove can effectively power five light-emitting diodes, indicating high potentials for future wearable smart textiles.

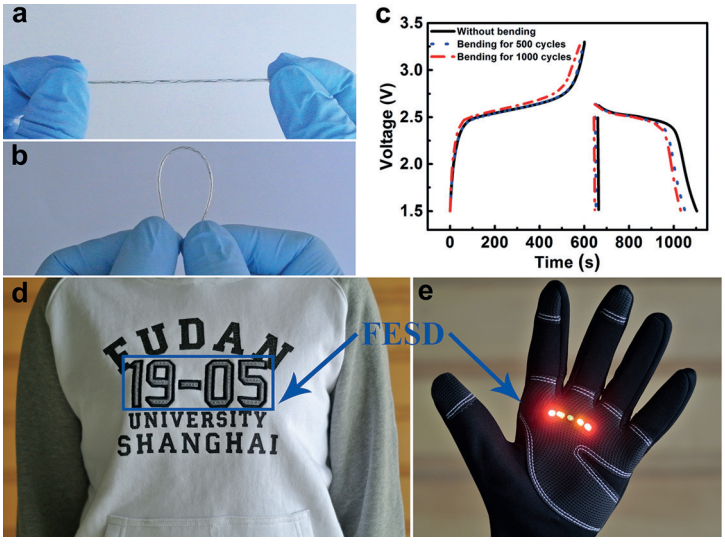

Figure 5. Flexibility and weaveability of the FESD. a),b) Photographs of an FESD before and after bending, respectively. c) The charge and discharge curves of an FESD before and after bending for 500 and 1000 cycles. d) Photograph of the FESD woven into a knitted sweater as the symbol "19-05". e) Photograph of the FESD woven into a glove to power five light-emitting diodes.

In summary, a novel FESD that combines the advantages of LIB and supercapacitor has been achieved by designing a three-electrode configuration. The FESD has shown both high energy and power densities, and the LIB and supercapacitor segments can be effectively operated together to reach remarkable energy storage and output. The FESDs are lightweight and flexible, and can be woven into various flexible electronic clothes. This work also offers a general and efficient route to develop high-performance miniature devices based on the design of multiple one-dimensional electrodes.

Acknowledgements

This work was supported by MOST (2011CB932503), NSFC (21225417), STCSM (12nm0503200, 15XD1500400), the Fok Ying Tong Education Foundation, the Program for Special Appointments of Professors at Shanghai Institutions of Higher Learning, and the Program for Outstanding Young Scholars from the Organization Department of the CPC Central Committee.

Keywords: carbon nanotubes · energy storage · fibers · hybrid device · wearable electronics

How to cite: *Angew. Chem. Int. Ed.* **2015**, *54*, 11177–11182
Angew. Chem. **2015**, *127*, 11329–11334

[1] J. Smithyman, Q. H. Do, C. Zeng, Z. Liang, *J. Power Sources* **2015**, *277*, 59–63.
[2] J. Huang, P. Xu, D. Cao, X. Zhou, S. Yang, Y. Li, G. Wang, *J. Power Sources* **2014**, *246*, 371–376.
[3] Z. Chen, V. Augustyn, J. Wen, Y. Zhang, M. Shen, B. Dunn, Y. Lu, *Adv. Mater.* **2011**, *23*, 791–795.
[4] X. Q. Wang, C. F. Wang, Z. F. Zhou, S. Chen, *Adv. Opt. Mater.* **2014**, *2*, 652–662.
[5] C. Yan, W. Kang, J. Wang, M. Cui, X. Wang, C. Y. Foo, K. J. Chee, P. S. Lee, *ACS Nano* **2014**, *8*, 316–322.
[6] H. M. Lee, S. Y. Choi, A. Jung, S. H. Ko, *Angew. Chem. Int. Ed.* **2013**, *52*, 7718–7723; *Angew. Chem.* **2013**, *125*, 7872–7877.
[7] R. J. Hamers, *Nature* **2001**, *412*, 489–490.
[8] M. Melzer, M. Kaltenbrunner, D. Makarov, D. Karnaushenko, D. Karnaushenko, T. Sekitani, T. Someya, O. G. Schmidt, *Nat. Commun.* **2015**, DOI: 10.1038/ncomms7080.
[9] M. Melzer, J. I. Mönch, D. Makarov, Y. Zabila, G. S. Cañón Bermúdez, D. Karnaushenko, S. Baunack, F. Bahr, C. Yan, M. Kaltenbrunner, *Adv. Mater.* **2014**, *27*, 1274–1280.
[10] L. Zhou, H. Y. Xiang, S. Shen, Y. Q. Li, J. D. Chen, H. J. Xie, I. A. Goldthorpe, L. S. Chen, S. T. Lee, J. X. Tang, *ACS Nano* **2014**, *8*, 12796–12805.
[11] K. Takei, W. Honda, S. Harada, T. Arie, S. Akita, *Adv. Healthcare Mater.* **2014**, *24*, 3299–3304.
[12] R. Li, B. Nie, P. Digiglio, T. Pan, *Adv. Funct. Mater.* **2014**, *24*, 6086–6086.
[13] T. Yamada, Y. Hayamizu, Y. Yamamoto, Y. Yomogida, A. Izadi-Najafabadi, D. N. Futaba, K. Hata, *Nat. Nanotechnol.* **2011**, *6*, 296–301.
[14] J. Ren, Y. Zhang, W. Bai, X. Chen, Z. Zhang, X. Fang, W. Weng, Y. Wang, H. Peng, *Angew. Chem. Int. Ed.*

2014, *53*, 7864 – 7869; *Angew. Chem.* **2014**, *126*, 7998 – 8003.
[15] Y. H. Kwon, S. W. Woo, H. R. Jung, H. K. Yu, K. Kim, B. H. Oh, S. Ahn, S. Y. Lee, S. W. Song, J. Cho, H. C. Shin, J. Y. Kim, *Adv. Mater.* **2012**, *24*, 5192 – 5197.
[16] X. L. Dong, Z. Y. Guo, Y. F. Song, M. Y. Hou, J. Q. Wang, Y. G. Wang, Y. Y. Xia, *Adv. Funct. Mater.* **2014**, *24*, 3405 – 3412.
[17] Y. Zhang, W. Bai, X. Cheng, J. Ren, W. Weng, P. Chen, X. Fang, Z. Zhang, H. Peng, *Angew. Chem. Int. Ed.* **2014**, *53*, 14564 – 14568; *Angew. Chem.* **2014**, *126*, 14792 – 14796.
[18] Y. N. Meng, Y. Zhao, C. G. Hu, H. H. Cheng, Y. Hu, Z. P. Zhang, G. Q. Shi, L. T. Qu, *Adv. Mater.* **2013**, *25*, 2326 – 2331.
[19] S. Brutti, V. Gentili, P. Reale, L. Carbone, S. Panero, *J. Power Sources* **2011**, *196*, 9792 – 9799.
[20] Z. Chen, D. Q. Zhang, X. L. Wang, X. L. Jia, F. Wei, H. X. Li, Y. F. Lu, *Adv. Mater.* **2012**, *24*, 2030 – 2036.
[21] M. D. Lima, N. Li, M. J. De Andrade, S. Fang, J. Oh, G. M. Spinks, M. E. Kozlov, C. S. Haines, D. Suh, J. Foroughi, *Science* **2012**, *338*, 928 – 932.
[22] W. H. Guo, C. Liu, F. Y. Zhao, X. M. Sun, Z. B. Yang, T. Chen, X. L. Chen, L. B. Qiu, X. H. Hu, H. S. Peng, *Adv. Mater.* **2012**, *24*, 5379 – 5384.
[23] L. Cheng, X. L. Li, H. J. Liu, H. M. Xiong, P. W. Zhang, Y. Y. Xia, *J. Electrochem. Soc.* **2007**, *154*, A692 – A697.
[24] Y. Y. Liang, S. J. Bao, B. L. He, W. J. Zhou, H. L. Li, *J. Electrochem. Soc.* **2005**, *152*, A2030 – A2034.
[25] H. Tang, Z. Chang, H. Zhao, X. Yuan, H. Wang, S. Gao, *J. Alloys Compd.* **2013**, *566*, 16 – 21.
[26] D. Pech, M. Brunet, H. Durou, P. Huang, V. Mochalin, Y. Gogotsi, P. L. Taberna, P. Simon, *Nat. Nanotechnol.* **2010**, *5*, 651 – 654.
[27] L. Kou, T. Huang, B. Zheng, Y. Han, X. Zhao, K. Gopalsamy, H. Sun, C. Gao, *Nat. Commun.* **2014**, DOI: 10.1038/ncomms4754.
[28] D. Yu, K. Goh, H. Wang, L. Wei, W. Jiang, Q. Zhang, L. Dai, Y. Chen, *Nat. Nanotechnol.* **2014**, *9*, 555 – 562.
[29] X. Xiao, T. Li, P. Yang, Y. Gao, H. Jin, W. Ni, W. Zhan, X. Zhang, Y. Cao, J. Zhong, *ACS Nano* **2012**, *6*, 9200 – 9206.
[30] Y. Yang, S. Jeong, L. Hu, H. Wu, S. W. Lee, Y. Cui, *Proc. Natl. Acad. Sci. USA* **2011**, *108*, 13013 – 13018.

Received: July 4, 2015
Published online: August 6, 2015